






## ORIGINAL ARTICLE

# Electric field promoted odontogenic differentiation of stem cells from apical papilla by remodelling cytoskeleton

Xiaolin Li<sup>1,2</sup>  | Sanjun Zhao<sup>3</sup> | Yao Liu<sup>4</sup>  | Yu Gu<sup>5,6</sup> | Lihong Qiu<sup>1</sup> | Xu Chen<sup>2</sup>  | Alastair J. Sloan<sup>2,7</sup>  | Bing Song<sup>8,9,10,11</sup> 

<sup>1</sup>Department of Endodontics, School and Hospital of Stomatology, Liaoning Provincial Key Laboratory of Oral Diseases, China Medical University, Shenyang, China

<sup>2</sup>Department of Pediatric Dentistry, School and Hospital of Stomatology, Liaoning Provincial Key Laboratory of Oral Diseases, China Medical University, Shenyang, China

<sup>3</sup>School of Life Sciences, Yunnan Normal University, Kunming, China

<sup>4</sup>Shanghai Engineering Research Center of Tooth Restoration and Regeneration & Tongji Research Institute of Stomatology & Department of Pediatric Dentistry, Shanghai Tongji Stomatological Hospital and Dental School, Tongji University, Shanghai, China

<sup>5</sup>Morrello Clinic, Neuro Rehabilitation and Neuro Physiotherapy, Newport, United Kingdom

<sup>6</sup>Cardiff Institute of Tissue Engineering and Repair, School of Dentistry, Cardiff University, Cardiff, United Kingdom

<sup>7</sup>Faculty of Medicine Dentistry and Health Sciences, Melbourne Dental School, University of Melbourne, Melbourne, Victoria, Australia

<sup>8</sup>Department of Dermatology, The First Hospital of China Medical University, National Health Commission key Laboratory of Immunodermatology, Key Laboratory of Immunodermatology of Ministry of Education, Shenyang, China

<sup>9</sup>School of Biomedical Engineering, Shenzhen University of Advanced Technology, Shenzhen, China

<sup>10</sup>Center for Translational Medicine Research and Development, Institute of Biomedical and Health Engineering, Shenzhen Institutes of Advanced Technology, Chinese Academy of Sciences, Shenzhen, China

<sup>11</sup>Key Laboratory of Biomedical Imaging Science and System, Chinese Academy of Sciences, and State Key Laboratory of Biomedical Imaging Science and System, Shenzhen, China

## Correspondence

Bing Song, Department of Dermatology, The First Hospital of China Medical University, National Health Commission Key Laboratory of Immunodermatology, Key Laboratory of Immunodermatology of Ministry of Education, Shenyang, China.  
Email: [songb3@cardiff.ac.uk](mailto:songb3@cardiff.ac.uk)

Alastair J. Sloan, Xu Chen, Department of Pediatric Dentistry, School and Hospital of Stomatology, Liaoning Provincial Key Laboratory of Oral Diseases, China Medical University, Shenyang, China.  
Email: [alastair.sloan@unimelb.edu.au](mailto:alastair.sloan@unimelb.edu.au); [chenxu@cmu.edu.cn](mailto:chenxu@cmu.edu.cn)

## Abstract

**Aim:** This study examined the impact of direct current electric fields (DCEFs) on the biological properties of stem cells derived from the apical papilla (SCAP) and further elucidated the underlying mechanisms involved in odontogenic differentiation induced by DCEFs stimulation.

**Methodology:** The measurement of endogenous currents in wounded dentine was achieved using a non-invasive vibrating probe system. Two-dimensional (2D) and three-dimensional (3D) systems were developed to apply DCEFs of varying strengths. The migration direction and trajectories of SCAP within DCEFs were analysed using time-lapse imaging. Cell proliferation was assessed through Hoechst staining and the CCK-8 assay. Changes in cell morphology, arrangement, and polarization were examined using fluorescence staining. The odontogenic differentiation of SCAP in vitro was assessed using quantitative polymerase chain reaction (qPCR), western blot analysis, alkaline phosphatase staining, and Alizarin Red S staining. In vivo evaluation was conducted through Haematoxylin and eosin

This is an open access article under the terms of the [Creative Commons Attribution-NonCommercial-NoDerivs](https://creativecommons.org/licenses/by-nc-nd/4.0/) License, which permits use and distribution in any medium, provided the original work is properly cited, the use is non-commercial and no modifications or adaptations are made.

© 2025 The Author(s). *International Endodontic Journal* published by John Wiley & Sons Ltd on behalf of British Endodontic Society.

**Funding information**

National Natural Science Foundation of China, Grant/Award Number: T2350710233 82060355; the National Key R&D Program of China, Grant/Award Number: 2024YFF206402, 2023YFC2508200; Shenzhen Science and Technology Program, Grant/Award Number: JCYJ20220818101404009; China Scholarship Council, Grant/Award Number: CSC201908210295

staining, immunohistochemistry staining, and Sirius Red staining after transplantation experiments.

**Results:** Injured dentine demonstrated a significantly increased outward current, and DCEFs facilitated the migration of SCAP towards the anode. DCEFs at a magnitude of 100 mV/mm promoted SCAP proliferation, whereas DCEFs at 200 mV/mm enhanced both polarization and odontogenic differentiation of SCAP. The application of cytoskeletal polymerization inhibitors mitigated the odontogenic differentiation induced by DCEFs. In vivo studies confirmed that DCEFs promoted the differentiation of SCAP into odontoblast-like cells in an orderly arrangement, as well as the formation of collagen fibres and dentine-like tissue.

**Conclusions:** DCEFs of varying intensities exhibited an enhanced capacity for migration, proliferation, odontogenic differentiation, and polarization in SCAP. These findings provide substantial insights for the advancement of innovative therapeutic strategies targeting the repair and regeneration of immature permanent teeth and dentine damage.

**KEYWORDS**

stem cells from apical papilla, odontogenic differentiation, dentine regeneration, direct current electric fields, cytoskeleton

**INTRODUCTION**

Pulp regeneration is a promising and difficult field of research in the treatment of endodontic diseases in recent years (Sui et al., 2019). Through the combination of growth factors and scaffold materials, stem cells are induced to differentiate into dentine-pulp complex (Yasui et al., 2017), repairing damaged tissues and restoring physiological functions. However, there are problems with the irregular morphology of the regenerated dentine, insufficient tissue formation, and a limited amount of tubular dentine and polarized odontoblast-like cells (Huang et al., 2020; Jung et al., 2019). Hence, it is imperative to select an appropriate and feasible stem cell source and investigate an innovative modulating approach in order to address the aforementioned dilemma.

Stem cells from apical papilla (SCAP) are a subset of oral stem cells obtained from the apical papilla of immature permanent teeth and serve as progenitors for the formation of apical dentine. Excellent advantages presented by SCAP include sufficient sources, strong self-renewal capability, and multi-directional differentiation ability, making them one of the most dominant cell types suitable for dentine regeneration (Ding et al., 2010; Huang et al., 2009). Recent studies have revealed that the arrangement pattern of odontoblasts has the potential to directly impact the function of odontoblast-like cells and subsequent secretion of dentine matrix (Yin et al., 2021). Therefore, improving the efficiency of SCAP differentiation into odontoblasts and formation of a palisade-like structure, with the aim of facilitating the

regeneration of adequate and well-organized tubular dentine, has become a topical challenge. A potential solution is the pre-odontogenic differentiation of transplants under optimized conditions with bioengineering strategies. The environment of stem cells in vivo consists of various extracellular matrix (ECM) components and signalling molecules, as well as physical, chemical, and biological factors that collectively influence the self-renewal and targeted differentiation of stem cells. Moreover, increasing evidence suggests that physical cues, such as mechanical forces, geometric properties, and electric signals, play a significant role in this process (Han et al., 2014; Xie et al., 2023). Endogenous electric fields are widely prevalent during embryonic development and the processes of tissue repair and regeneration and could regulate cellular functions including cell migration, proliferation, and differentiation (Leppik et al., 2020). However, there is still limited understanding regarding the effects and mechanisms of direct current electric fields (DCEFs) maintained in the physiological range on the differentiation of stem cells into odontoblast-like cells.

In this study, wound-induced endogenous electric currents were directly measured on damaged dentine of human teeth. Two-dimensional (2D) and three-dimensional (3D) DCEFs stimulating models in vitro and a root fragment model in vivo were constructed to mimic the effects of endogenous wound current on the directional migration, proliferation, and odontogenic differentiation of SCAP, and to determine whether DCEFs promote odontogenic differentiation of SCAP by remodelling the cytoskeleton. To the best of our knowledge, this

is the first study clarifying the electrotaxis of SCAP in the process of odontogenic differentiation and providing a basis and theoretical rationale for further application of DCEFs of tubular dentine regeneration in pulp-dentine complex repair (Figure 1).

## MATERIALS AND METHODS

The manuscript of this laboratory study has been written according to Preferred Reporting Items for Laboratory studies in Endodontology (PRILE) 2021 guidelines (Nagendrababu et al., 2021). The research methodology and principal findings are presented in Figure 2.

### Isolation and culture of SCAP

This study was approved by the Ethics Committee of the School and Hospital of Stomatology, China Medical University (No. 201315). SCAP were isolated from the apical papilla of human immature tooth roots as previously described (Liu et al., 2021). Briefly, the tissue was washed with phosphate-buffered saline (PBS, Gibco, Grand Island, NY, USA), digested with 3 mg/mL collagenase type I (Sigma-Aldrich, St. Louis, MO, USA) and 4 mg/mL dispase II (Sigma-Aldrich) at 37°C for 30 min, then strained through a 70 µm cell strainer to obtain single-cell suspensions. The cells were seeded in a T25 culture flask with alpha minimum essential medium (α-MEM, Gibco) supplemented with 10% foetal bovine serum (FBS, Gibco) and 100 U/mL penicillin–streptomycin (Gibco). To identify SCAP, osteoblastic, chondrogenic, and adipogenic differentiation ability and cell surface markers were determined.

Passage 3–5 of SCAP were used for subsequent experiments. After the confluence reached 80%, culture medium

was substituted with osteogenic/odontogenic differentiation medium, comprising 10% foetal bovine serum (Gibco), 1% Penicillin–Streptomycin solution (Gibco), 50 µg/mL L-ascorbic acid 2-phosphate (L-ASA, Sigma-Aldrich), 10 mM β-Sodium glycerophosphate hydrate (Sigma-Aldrich), and 100 nM dexamethasone (Sigma-Aldrich). Subsequent experiments under DCEFs were performed after 14 days of osteogenic/odontogenic differentiation. After 14 days of osteogenic/odontogenic differentiation, subsequent experiments under DCEFs were performed after this step. SCAP were treated with the microtubule polymerization inhibitor Nocodazole (10 µM, MedChem Express, Monmouth Junction, NJ, USA), the myosin polymerization inhibitor Blebbistatin (10 µM, MedChem Express) or the Rho-associated coiled-coil-containing protein kinase (ROCK) inhibitor Y27632 (10 µM, MedChem Express) to reduce the effect of cytoskeletal polymerization before the stimulation of DCEFs.

### Osteogenic differentiation assay

After SCAP were cultured in osteogenic/odontogenic differentiation medium for 21 days, Alizarin Red S (ARS, Sigma-Aldrich) staining was performed. For semi-quantification, the mineralised nodules were solubilized using a 10% solution of cetylpyridinium chloride (CPC, Sigma-Aldrich) and the absorbance OD value was measured at 562 nm.

### Chondrogenic differentiation assay

To evaluate the capacity to differentiate into chondrocytes, SCAP were incubated in chondrogenic differentiation medium (Cyagen, Guangzhou, China) in 15 mL

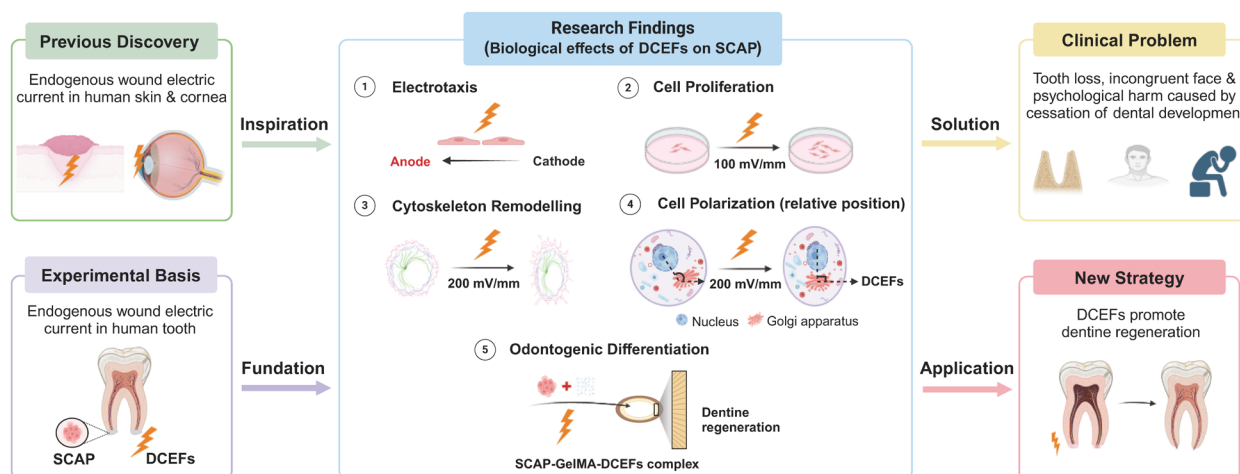


FIGURE 1 Schematic illustration of the experimental design. Created with BioRender.com.



**FIGURE 2** PRILE 2021 flowchart outlining the methodology and principal findings involved in this study.

centrifuge tubes. After 28 days, the formed pellets were fixed in 4% paraformaldehyde (Boster, Wuhan, China) and subjected to dehydration via sucrose gradient.

Frozen sections (10 µm) obtained by cryosectioning (Leica, Wetzlar, Germany) were stained with toluidine blue (Cyagen).



## Adipogenic differentiation assay

The adipogenic differentiation of SCAP was induced with adipogenic induction and maintenance differentiation medium (Cyagen) for a duration of 30 days. Subsequently, lipid accumulation was visualized through the application of Oil red O staining (Sbjbio, Nanjing, China).

## Flow cytometry for surface markers analysis

Single cell suspension of SCAP ( $1 \times 10^6$ /mL) was incubated with fluorescein isothiocyanate (FITC)-conjugated antibodies against human CD44, CD105, CD34, and CD45, and phycoerythrin (PE)-conjugated antibodies against human CD90 and CD146 (1:1000, eBioscience, San Diego, CA, USA) at 4°C for 1 h. Then SCAP were washed with PBS and analysed with a flow cytometer (Becton Dickinson, Franklin Lakes, NJ, USA) and FlowJo (V10.10.0, TreeStar, Ashland, OR, USA).

## Establishment of DCEFs application system

The application system of DCEFs was designed following the previously described methodology (Song et al., 2007), including four components: a DC regulated power supply (Aim, Huntingdon, UK), silver/silver chloride electrodes, a conducting liquid pool (Steinberg's solution), and an electrical stimulation chamber. The power supply and electrode were connected through the wire, whilst the electrode and cell were connected through the conductive liquid pool. The direct current was transmitted through the positive electrode of the power supply and formed a closed circuit through the wire, electrode, conductive liquid pool, salt bridge, cell, salt bridge, conductive liquid pool, electrode and negative electrode of the power supply. The cover glasses (Citotest, Nantong, China) were used to create a  $20 \times 10 \times 0.2$  mm chamber with high vacuum silicone grease (Dow Corning, Midland City, MI, USA) in a sterile 100 mm cell culture petri dish and the area for cell seeding was  $2 \text{ cm}^2$ . After SCAP were seeded in the designed area for 12 h, a cover glass ( $20 \times 20$  mm, Citotest) was used for sealing the cell culture chamber with high vacuum silicone grease. Silver/silver chloride electrodes were connected to both sides of cell seeding area by a pair of 2% agar powder-Steinberg's solution bridges, aiming at minimizing the cytotoxic effects resulting from electrolysis products during the stimulation of DCEFs and confining DCEFs only through the cell culture chamber (Figure S2a,b).

The 3D application system of DCEFs was modified with 5% (w/v) concentration of porous gelatine methacrylate (GelMA) hydrogel (EFL, Suzhou, China) (Khayat et al., 2017). SCAP were encapsulated within GelMA at a concentration of  $3 \times 10^6$  cells/mL, and subsequently, a volume of  $20 \mu\text{L}$  cell-laden hydrogel was dropped on the designated region of the specific DCEFs-stimulation dish. The hydrogel was then cured using a 405 nm light source (EFL) for a duration of 10 s. After 24 h, the cells were observed to exhibit spreading behaviour under microscopic examination. For further detection, a GelMA lysis solution (0.3 mg/mL, EFL) was added into an Eppendorf tube and incubated at 37°C for 1 h. Subsequently, centrifugation at 1000 rpm for 5 min was performed to dissociate the GelMA.

## Electrotaxis detection

The DC voltage level of the multimeter (Kane, Welwyn Garden City, UK) was measured at 2 V, 4 V, and 6 V by systematically adjusting the output of the DC power supply and the resistance of the rheostat per hour, ensuring a steady intensity of 100 mV/mm, 200 mV/mm, or 300 mV/mm for a duration of 8 h. The petri dish was transferred to a clean enclosure for the microscope (PureBox Shiraito, Fujinomiya City, Japan) at 37°C for 8 h under the stimulation of DCEFs. Time-lapse images of 5 min/frame for the X and Y axes were recorded through the IXplore SpinSR confocal microscope system (Olympus, Tokyo, Japan). Data processing and analysis of the collected images were performed by ImageJ software (v.1.8.0, National Institutes of Health, NIH, Bethesda, MD, USA).

The motility of cells in DCEFs was assessed by migration speed, migration efficiency, X-axis translocation, and directedness. Migration speed was utilized to quantify the velocity of SCAP, whilst migration efficiency was employed to measure the actual effectiveness of the straight-line distance covered by SCAP from the starting point to the endpoint. Directedness was utilized to ascertain the migration direction, with a value of "0" indicating random migration, "1" indicating directed movement towards the cathode, and "-1" indicating directed movement towards the anode (Figure S2c).

## Proliferation assays

The immediate effect of DCEFs on the proliferation of SCAP was detected by Hoechst 33342 staining. Briefly, Hoechst 33342 working solution (0.1 mg/mL, Selleck, Houston, TX, USA) was added 20 min before time-lapse imaging, which was captured from five independent sites per group. After the stimulation of DCEFs, the total count of Hoechst

33342-positive cells in the 97th and 1st photographs from each site was counted with ImageJ software (v.1.8.0, NIH) and subsequently divided for statistical analysis.

The viability of SCAP was evaluated using the cell counting kit-8 (CCK-8, Dojindo, Kumamoto, Japan) assay to examine the long-term impact on various intensities of DCEFs. In detail, after exposure to DCEFs of 100 mV/mm, 200 mV/mm, or 300 mV/mm for 8 hours, the cells were seeded into the 48-well plates at a density of  $1 \times 10^4/\text{cm}^2$  and analysed on days 1, 3, 5, and 7, respectively. SCAP without DCEFs stimulation was set as the blank control group for each intensity of DCEFs and time point.

## Immunofluorescence and assays

SCAP that had undergone different treatments was fixed with 4% paraformaldehyde (Boster) for 15 min, permeabilised with 0.1% Triton X-100 (Beyotime Biotechnology, Shanghai, China) for 10 min, blocked with 1% BSA (Solarbio, Beijing, China) for 30 min at room temperature (RT), then incubated with primary antibody and corresponding secondary antibody. Cell nuclei were stained with 4', 6-diamidino-2-phenylindole (DAPI, Beyotime Biotechnology). The samples were visualized and photographed under a laser scanning confocal microscope (Olympus).

Phalloidin staining of F-actin was performed to detect the effect of DCEFs on the arrangement and morphology of SCAP. After conducting Phalloidin (Yeasen, Shanghai, China) and DAPI (Beyotime Biotechnology) staining, a total of 10 non-overlapping fields were used to determine the angle between the longitudinal axis of cells and the direction of the electric fields, as well as to measure the length and width. The ratio of width to length of SCAP was determined by comparing the shortest and longest lengths per cell, whereby a ratio of 1.0 indicated a perfectly round cell, whilst a ratio of 0.1 denoted a highly elongated cell. Angles exceeding  $90^\circ$  were adjusted to their corresponding acute angles for the purpose of statistical analysis.

Cell polarization analysis was measured as previously reported (Li et al., 2018). SCAP were stained with anti-GM130 antibody (1:3000, Cell Signalling Technology, Danvers, MA, USA) and DAPI (Beyotime Biotechnology) to visualize the relative positions of Golgi and the nucleus. Alexa Fluor 594 donkey anti-rabbit IgG (1:1000, Thermo Fisher Scientific Waltham, MA, USA) was used as the secondary antibody. Each cell was evenly divided into three sections with a central angle of  $120^\circ$ , and their classification as polarized or non-polarized was determined based on the location of their Golgi bodies. Specifically, cells were classified as polarized when Golgi bodies were situated in

the section perpendicular to the horizontal direction of DCEFs, whereas cells with Golgi bodies in any other section were considered unpolarised cells. The cell number was measured with ImageJ software (v.1.8.0, NIH).

## Alkaline phosphatase (ALP) staining and activity assay

ALP staining of SCAP was performed using the ALP colour development kit (Beyotime), and the ALP activity was quantitatively assessed using the ALP assay kit (Beyotime), following the manufacturer's instructions.

## Reverse transcription and quantitative polymerase chain reaction (qPCR)

Total RNA of cells was extracted with RNAiso Plus (Takara, Tokyo, Japan) and cDNA was obtained by reverse transcription reaction with PrimeScript RT reagent kit (Takara). qPCR was performed in at least 3 independent experiments with TB Green Premix Ex Taq II (Takara) in LightCycler 96 Instrument (Roche, Basel, Switzerland). The mRNA expression levels of dentine sialophosphoprotein (DSPP), dentine matrix protein 1 (DMP1) and ALP were evaluated with glyceraldehyde-3-phosphate dehydrogenase (GAPDH) as housekeeping gene for normalizing, and the data were calculated by the  $2^{-\Delta\Delta C_t}$  formula. The primer sequences synthesized by Sangon Biotech (Shanghai, China) are presented in Table S1.

## Western blot analysis

Total protein was extracted using radio immunoprecipitation assay (RIPA) lysis buffer (Thermo Fisher Scientific) with protease inhibitor cocktail (Beyotime Biotechnology) for 30 min on ice. Protein concentrations were detected by a BCA protein assay kit (Beyotime Biotechnology). Samples were boiled with  $5 \times$  loading buffer (Epizyme, Shanghai, China) for 10 min. Next, 30  $\mu\text{g}$  protein of each sample was loaded and separated by 7.5% sodium dodecyl sulphate polyacrylamide gel (Epizyme) electrophoresis and then transferred to 0.45  $\mu\text{m}$  polyvinylidene difluoride membranes (Merck Millipore, Billerica, MA, USA). The membranes were blocked in 3% BSA (Solarbio) at RT for 1 h and exposed to respective antibodies: anti-DSPP (1:500, Santa Cruz Biotechnology, Santa Cruz, CA, USA), anti-DMP1 (1:500, Santa Cruz Biotechnology), anti-ALP (1:500, Santa Cruz Biotechnology) or anti-GAPDH (1:20000, Abcam, Cambridge, MA, USA). Membranes

were incubated with the primary antibodies overnight at 4°C, and then with goat anti-rabbit/anti-mouse IgG horseradish peroxidase (HRP)-conjugated secondary antibody (1:10000, Abcam) for 1 h at RT. The protein bands were revealed with ChemiDoc MP Imaging System (Bio-Rad, Cambridge, MA, USA) and the grey value of each band was measured with ImageJ software (v.1.8.0, NIH) to quantify relative protein expression.

## Preparation of dentine wound and tooth slides

Healthy premolars extracted for orthodontic requirements were obtained from the Ethics Committee of the School and Hospital of Stomatology, China Medical University (No. G2018009). Soft tissues on the root surface were removed with a No. 10 surgical blade (Jinhuan Medical, Shanghai, China). For dentine wound preparation, fine high-speed zirconia cutting burs were used (Eagle Dent, Sialkot, Pakistan). For tooth slide preparation, 3 mm length root fragments close to the cervical of the teeth were intercepted, and then the cementum and dental pulp tissue were removed by high-speed handpieces (NSK, Tokyo, Japan) with fissure burs (Mani, Utsunomiya, Japan). The internal and external walls of each tooth segment were smoothed with a diamond bur (Mani) successively. Subsequently, all tooth fragments were subjected to immersion in a 1% sodium hypochlorite solution (Aladdin, Shanghai, China) and a 17% ethylenediaminetetraacetic acid solution (EDTA, Macklin, Shanghai, China) for a duration of 10 min. Following this, ultrasonic cleaning using sterile distilled water was performed for 5 min, prior to liquid replacement and as the concluding step for achieving cleanliness. All segments were sterilized by high temperature and high pressure after desiccation.

## Endogenous current measurement for wounded dentine

Wound-induced endogenous electric current measurements were conducted using a non-invasive vibrating probe system following the methodology outlined in previous studies (Reid et al., 2007). The probe was displaced approximately 50 µm from the surface at various measuring locations within wounded dentine. The current measurements were performed at the wound edge (c & g), wound centre (d-f) and distal site away from the wound (a, b, h, i). A minimum of three measurements were obtained at each measuring point and calculated. The total duration of measurement was 300 min.

## Transplantation experiments in vivo

This manuscript follows the Preferred Reporting Items for Animal Studies in Endodontology (PRIASE) 2021 guidelines. BALB/c-nu mice (male, 8 weeks old) were purchased from SiPeiFu Biotechnology (Beijing, China). All animal experiments were approved by the Institutional Animal Care and Use Committee of China Medical University (No. CMU2021211). All operations were performed under 1% isoflurane (Ringpu, Tianjin, China) gas anaesthesia (RWD, Shenzhen, China). The in vivo experiments were divided into 4 groups: empty control group, GelMA control group, SCAP-GelMA group, and SCAP-GelMA-DCEFs group ( $n=6$ ). GelMA with or without SCAP was introduced into tooth segments and transplanted subcutaneously into the backs of nude mice. Each mouse contained 4 different tooth segments, and there was no connection among them. Following an 8 weeks implantation period, the mice were sacrificed, and tooth segments were extracted for analysis.

## Haematoxylin and eosin (H&E) staining, Sirius red staining, and immunohistochemistry (IHC) staining

Root fragment samples harvested from mice were fixed in 4% paraformaldehyde (Boster) for 72 h, and then decalcified in a 10% EDTA decalcifying solution (Boster) for 3 months. The decalcified root fragments were embedded in paraffin and cut into sections of 3 µm thickness. Sections were deparaffinized and rehydrated through a graded xylene and alcohol series, and then stained with an H&E staining kit (Beyotime Biotechnology). The number of odontoblast-like cells beside the internal dentinal walls of the tooth fragments was measured using ImageJ software (v.1.8.0, NIH).

Sirius red staining was performed to detect the distribution and arrangement of collagen fibres according to the instructions (Abcam), indicating that collagen I was shown in red or orange, whilst collagen III was shown in green or yellow. Bright-field and polarized images were taken with a whole slide scanner (SLIDEVIEW VS200, Olympus).

For IHC staining, anti-DSPP antibody (1:200, Santa Cruz Biotechnology), anti-DMP1 antibody (1:200, Santa Cruz Biotechnology) and DAB detection kit (Gene Tech, Shanghai, China) were used according to the manufacturer's protocol. The quantification of immunohistochemistry was accessed by calculating the relative integrated optical density (IOD)/area using Image-Pro Plus 6.0 software (Media Cybernetics, Silver Springs, MD, USA).

## Statistical analysis

GraphPad Prism (Version 8.0, La Jolla, CA, USA) was employed for statistical testing and plotting. All data were obtained from at least three independent experiments and were presented as mean  $\pm$  standard deviation (*SD*). Statistical comparisons between data sets were performed with the analysis of normality and variance. Statistical analysis involved the use of Student's *t* test for comparisons between two groups and one-way analysis of variance (ANOVA) for multiple comparisons. Statistical significance was considered as  $p < .05$ .

## RESULTS

### Endogenous electrical current in wounded dentine

The schematic plot of current measurement in wounded dentine of human tooth is shown in [Figure 3a](#). The results indicated that wounds exhibited a significantly greater outward current, as depicted in [Figure 3b](#). Specifically, the current at the periphery of the wound (positions “c” and “g”) was found to be higher than at the centre of the wound (position “e”). Time course experiments conducted on dentine wounds revealed that the current at the wound edge progressively increased from the initial time of injury, reaching a peak after 100 min before stabilizing ([Figure 3c](#)).

### Different strengths of DCEFs affected electrotaxis and cell proliferation of SCAP

First, we isolated SCAP from apical papilla and identified the surface markers and multiple differentiation abilities of SCAP ([Figure S1](#)). In the absence of DCEFs, the migration directedness of SCAP was observed to be close to the origin of coordinates, indicating a random movement pattern ([Figure 3d](#), [Movie S1a](#)). Conversely, the introduction of DCEFs induced a distinct electrotactic response of SCAP, resulting in a directional movement towards the anode ([Figure 3e–gk](#) and [Movie S1b](#)). Further analysis of time-lapse recordings revealed that the electrotactic response of SCAP reached its maximum at 200 mV/mm DCEFs, resulting in enhanced migration velocity, migration efficacy, X-axis translocation, and migration directedness approaching “1” when compared to alternative approaches ([Figure 3h–j](#)).

Hoechst 33342 staining was employed as a quantitative measure to evaluate cell proliferation in an intuitive manner, whilst the CCK-8 assay was utilized for

semi-quantitative evaluation of cell proliferation in response to DCEFs stimulation. The experimental findings demonstrated that DCEFs at a magnitude of 100 mV/mm significantly enhanced the proliferation of SCAP. Conversely, DCEFs at 200 mV/mm did not exert a significant impact on proliferation. Notably, DCEFs at 300 mV/mm inhibited cell proliferation compared to SCAP that were not subjected to stimulation ([Figure 3l,m](#)).

### DCEFs remodelled the cytoskeleton of SCAP

By employing phalloidine staining to visualize F-actin, SCAP of control groups exhibited a short spindle shape with irregular direction and arrangement. Following the application of DCEFs at a magnitude of 200 mV/mm, the previously disordered arrangement transformed into palisades perpendicular to the direction of the DCEFs ([Figure 4a](#)). Subsequent examination revealed that the cytoskeleton experienced predominantly remodelling in terms of cellular alignment and elongation. SCAP in the control group exhibited a relatively uniform distribution of the angle between the long axis and the horizontal direction, which was equivalent to the vector of DCEFs. Conversely, the DCEFs group exhibited a noticeable imbalance in this distribution, with approximately 67% of cells being nearly vertically aligned with the direction of DCEFs, a significantly higher proportion compared to the 12.5% of the control group ([Figure 4b](#)). Furthermore, the curve depicting the ratio of width to length of the cytoskeleton in the electrically stimulated group exhibited a notable leftward shift when compared to the control group. This shift indicated a negative correlation between the cytoskeletal ratio and cell elongation, suggesting that the application of DCEFs facilitated the elongation of SCAP ([Figure 4c](#)).

Next, the influence of cytoskeleton polymerization on cell motility, arrangement, and morphology under DCEFs was evaluated. SCAP displayed slower migration speed and efficiency under the effect of cytoskeletal polymerization inhibitors compared with the untreated group ([Figure 4d,e](#)), whereas the migration direction towards the anode was not altered ([Figure 4f,g](#)). The cells in the drug-treated group exhibited a stochastic arrangement, with a higher proportion of cells perpendicular to the direction of DCEFs post-stimulation, albeit lower than the group exclusively exposed to DCEFs ([Figure 4h](#)). Additionally, the width-to-length ratio of SCAP increased subsequent to pretreatment with Nocodazole, Blebbistatin, or Y27632, resulting in a displacement towards the right in the distribution curve ([Figure 4i–k](#), grey curve). Conversely, the width-to-length ratio of SCAP decreased and the



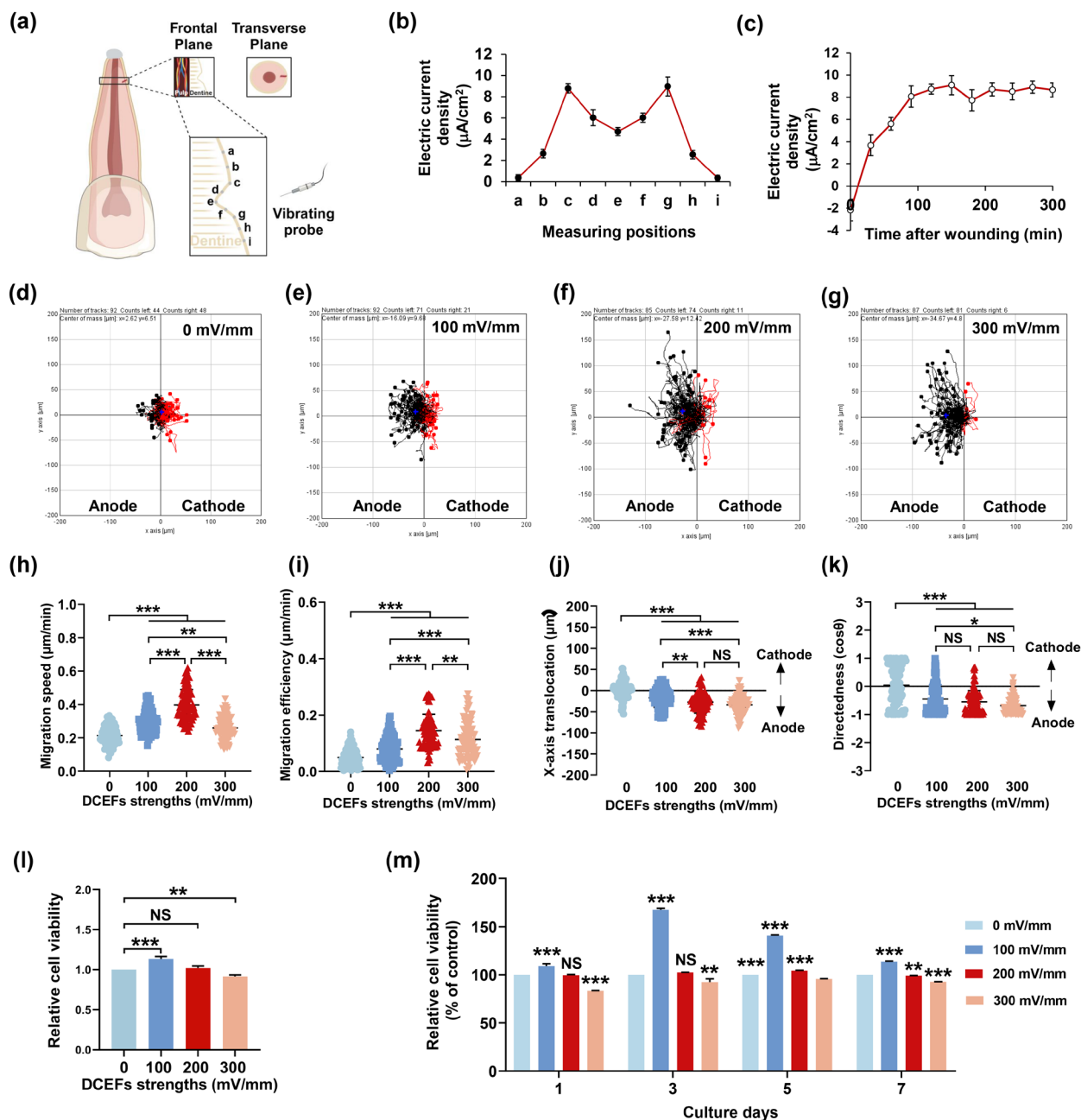


**FIGURE 3** DCEFs in physiological strength ranges affected electrotaxis and proliferation of SCAP. (a) Schematic diagram of the measurement at different positions by a vibrating probe. Grey dots indicated measuring positions “a” to “i”. (b) Upward peaks showed outward currents in damaged dentine. Maximum current was seen at the wound edges (positions “c” and “g”). (c) Changes of wound current in dentine over time. (d–g) Migration trajectories of SCAP in 0, 100, 200, 300 mV/mm DCEFs respectively. (h–j) Analysis of the migration speed, efficiency and X-axis translocation of SCAP under DCEFs of different intensity. (k) The SCAP exhibited directional migration towards the anode, and variations in field strength did not influence the directionality of this migration. (l) Assessment of immediate proliferation effect after 8 hours of DCEFs stimulation measured by Hoechst 33342 staining. (m) The relative cell viability of SCAP was measuring by CCK-8 assay (NS:  $p > .05$ , \* $p < .05$ , \*\* $p < .01$ , \*\*\* $p < .001$ ).

distribution curve shifted to the left (Figure 4i–k, red curve) when DCEFs were loaded subsequently. It is noteworthy that the distribution curves of inhibitor-pretreated groups remained predominantly on the right side of the DCEFs stimulation group (Figure 4i–k, blue curve), indicating DCEFs could partially rescue the

cellular rounding induced by inhibitors of cytoskeletal polymerization.

Collectively, these results demonstrated that DCEFs possess the ability to counteract the inhibitory impact of cytoskeletal protein polymerization inhibitors, thereby promoting cell elongation and reorientation.

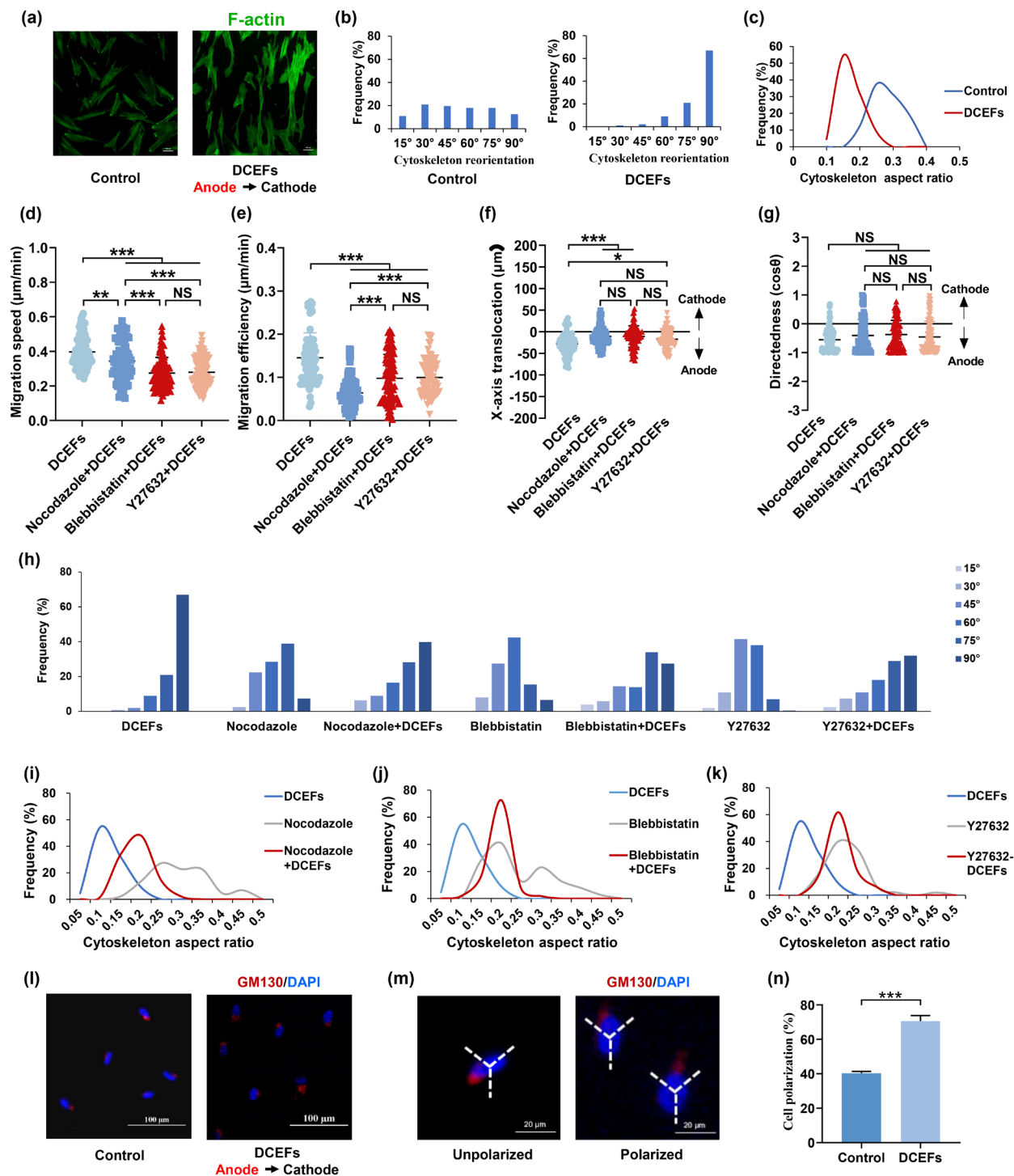


**FIGURE 4** DCEFs induced alterations in cell morphology, arrangement and polarization of SCAP. (a, b) Fluorescent images and histograms revealed SCAP were disordered without DCEFs stimulation whilst regularly aligned after 200 mV/mm DCEFs stimulation respectively (black arrow: the direction of DCEFs, green: F-actin stained by phalloidin, scale bar = 100  $\mu$ m). (c) The width-to-length ratio of DCEFs group was generally lower compared to that of the control group in distribution diagram. (d, e) Nocodazole, Blebbistatin and Y27632 decreased the migration speed and efficiency of SCAP. (f, g) Cytoskeletal polymerization inhibitors showed no significant effect on X-axis translocation and migration direction of SCAP in DCEFs. (h) Distribution of the cell axis at angles with the direction of DCEFs. (i–k) The increase in width-to-length ratio of SCAP induced by cytoskeletal polymerization inhibitors was partially mitigated by DCEFs. (l) Relative position of the cell nucleus and Golgi apparatus of SCAP with and without the stimulation of DCEFs (black arrow: the direction of DCEFs, blue: cell nucleus, red: Golgi apparatus, scale bar = 100  $\mu$ m). (m) Schematic illustration of the definitions for unpolarised and polarised cells (blue: cell nucleus, red: Golgi apparatus, white dotted lines: the lines of equality of 120°, scale bar = 20  $\mu$ m). (n) Cell polarization ratio analysis (NS:  $p > .05$ , \* $p < .05$ , \*\* $p < .01$ , \*\*\* $p < .001$ ).

## DCEFs facilitated SCAP polarization

To further explore the role of DCEFs in the modification of critical organelles, immunofluorescence staining was employed to analyse the changes in the relative positioning of the Golgi apparatus and nucleus following stimulation with DCEFs. Fluorescent imaging revealed a significant increase in cellular polarization subsequent to the stimulation of DCEFs, as evidenced by an elevated proportion of cells exhibiting the Golgi apparatus positioned directly above or below the nucleus (Figure 4l,m). Specifically, the cell polarization ratio was  $40.3\% \pm 0.9\%$  in the control group, whereas it reached  $70.6\% \pm 2.6\%$  in the DCEFs stimulation group (Figure 4n).

## DCEFs improved the odontogenic differentiation ability of SCAP in vitro

Given the aforementioned data, which have elucidated the crucial involvement of DCEFs in governing diverse cellular processes including migration, proliferation, arrangement, shape, and polarization, we proceeded to assess the influence of DCEFs on odontogenic differentiation. Notably, the application of 200 mV/mm DCEFs resulted in a significant increase in both ALP activity and mineralised nodule formation (Figure 5a–d). Furthermore, to examine the influence of cell morphology and alignment on SCAP odontogenesis, we subsequently assessed the expression of key odontogenic marker genes and proteins in cells that were pre-treated with Nocodazole, Blebbistatin, and Y27632, followed by exposure to 200 mV/mm DCEFs. A substantial up-regulation of *DSPP*, *DMP1*, and *ALP* gene expression was observed in DCEFs-treated groups compared with that in the control group (Figure 5e–g). Additionally, a similar up-regulation was observed in the inhibitor-pretreated under DCEFs groups compared to the respective inhibitor-treated group. Meanwhile, the protein expression levels of DSPP, DMP1, and ALP were consistent with the qPCR results (Figure 5h–k). The results obtained clearly demonstrate the effective stimulation and counteraction of DCEFs on the suppressive impact of cytoskeletal polymerization inhibitors on the expression of dentine-related genes and proteins in SCAP.

## DCEFs boosted dentinogenesis of SCAP in vivo

A 3D culture and DCEFs-loading system was established with the intention of conducting subsequent animal experiments (Figure 6a and Figure S3). Firstly, we tested the dentinogenesis ability of SCAP in the 3D system. The

results revealed that DCEFs exhibited a notable influence on the mRNA and protein levels of DSPP, DMP1, and ALP (Figure S3). The effects of DCEFs on dentin formation in vivo were investigated by implantation of tooth fragments containing the SCAP-GelMA complex into the back of nude mice. Compared with the empty control group and the GelMA control group, the SCAP-GelMA group and the SCAP-GelMA-DCEFs group exhibited a stronger bond between the newly formed tissue and the internal dentin layer of the root fragment. More importantly, the nuclei of odontoblast-like cells were observed to be arranged at the interface between the newly developed soft tissue and the dentinal walls of the canal (Figure 6b). The findings from the quantitative analysis revealed a higher presence of odontoblast-like cells in the SCAP-GelMA-DCEFs group as compared to the others (Figure 6f).

Another promising finding arose from Sirius red staining, a method employed to assess the composition, organization, and maturity of collagen fibres in dentine. Specifically, the collagen fibres exhibited birefringence when observed through a polariscope, with type I collagen fibres displaying a vibrant orange or red hue, whilst type III collagen fibres exhibited a green coloration. Results showed the inner wall of the root fragments in both the empty control group and the GelMA control group consistently exhibited a bright orange-red colour, suggesting a heightened level of light refraction and less light penetration under polarized light irradiation. On the contrary, irregular, dark, and thin layers were observed adjacent to the inner wall of the root fragments in the SCAP-GelMA and SCAP-GelMA-DCEFs groups (Figure 6c). These layers mainly consisted of type I collagen, with a minor presence of type III collagen, as indicated by reduced refraction and increased penetration under polarized light irradiation, indicating the formation of newly regenerated collagen fibres.

The regenerated tissues were further analysed by immunohistochemistry with DSPP and DMP1 as markers specific to odontogenesis. Positive staining for DSPP and DMP1 was observed in the SCAP-GelMA group and SCAP-GelMA-DCEFs group, suggesting that the differentiated odontoblast-like cells were responsible for the production of the dentine-like tissues (as indicated by yellow arrows, Figure 6d,e,g,h).

## DISCUSSION

Pulpitis and apical periodontitis are the most prevalent dental diseases, characterized by inflammation and destruction of pulpal and periapical tissues (Tibúrcio-Machado et al., 2021). Particularly, damage to dentine tissue in the apical area often causes the arrest of tooth

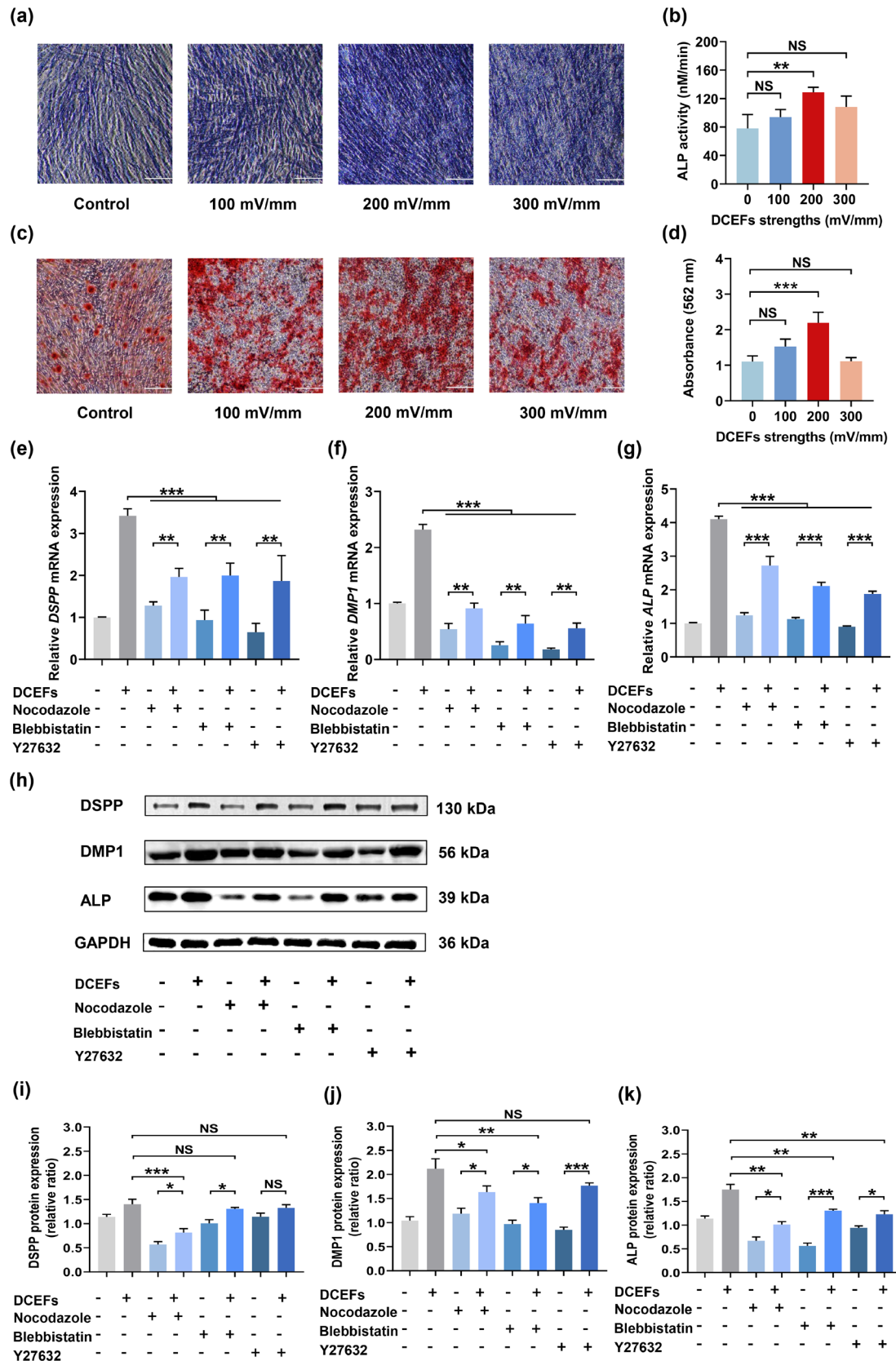


**FIGURE 5** DCEFs improved odontogenic differentiation ability of SCAP in vitro. (a, b) 200 mV/mm DCEFs significantly increased ALP expression of SCAP (scale bar = 200  $\mu$ m). (c, d) Alizarin red S staining showed that DCEFs could increase mineralised nodule formation with the highest effect at a magnitude of 200 mV/mm (scale bar = 200  $\mu$ m). (e–k) DCEFs partially recovered the decreased mRNA and protein expression of DSPP, DMP1 and ALP induced by cytoskeletal polymerization inhibitors (NS:  $p > .05$ , \* $p < .05$ , \*\* $p < .01$ , \*\*\* $p < .001$ ).



root development and increases the difficulty of cure. Thus, the primary objective of mesenchymal stem cells (MSCs)-based tissue engineering is the regeneration of functional dentine. SCAP, being dentine tissue-specific, show promise as potential candidates for dentine regeneration and bio-root engineering due to their unique ability to differentiate into odontoblasts during dentine development (Piva et al., 2014). However, additional research is necessary to overcome challenges associated with current pulp regeneration strategies, including inadequate and irregular morphology of dentine formation. The utilization of DCEFs to aid in wound healing, which underpins Medicare-approved electrical stimulation therapy, has established the importance of biophysical factors in regulating various cellular responses (Grimm et al., 2014).

Our research initially detected endogenous currents in injured teeth with the goal of deducing the strength of DCEFs in the physiological range, which is usually smaller than 500 mV/mm (Al Hezaimi et al., 2023; Balmer et al., 2018; Hart & Palisano, 2017). A prior study demonstrated that DCEFs consistently range from 100 to 150 mV/mm during the wound healing process, persisting for several hours or days until epithelial cells fully covered the wound (McCaig et al., 2005). A lower intensity of electrical stimulation can prompt soft tissue cells to initiate signal transduction processes associated with regeneration (Chen et al., 2019). In contrast, cells involved in hard tissue formation demonstrate a higher threshold for electrical stimulation due to the rigid extracellular matrix components like collagen and hydroxyapatite, which hinder electrical signal transmission. Consequently, a greater current intensity is required to activate the regeneration-related physiological processes in hard tissue cells compared to those in soft tissue formation. Intensities of DCEFs in 400 and 500 mV/mm were found to make cells rapidly become poorly functional (data not shown). Taken together, we chose the intensities of 100, 200, and 300 mV/mm to detect the modulation of DCEFs on SCAP functionality. We demonstrated that DCEFs with an intensity of 200 mV/mm significantly enhanced the odontogenic differentiation capability of SCAP in both 2D and 3D culture systems. Additionally, we developed an experimental model to validate the efficacy of electrical stimulation, revealing that SCAP differentiated into odontoblast-like cells with a well-organized arrangement, thus highlighting the crucial role of DCEFs in promoting odontogenesis.

Numerous studies have demonstrated that under pathological conditions or external injury, the pulp-dentine complex can be repaired through the proliferation, differentiation, and migration of SCAP to achieve tissue regeneration (Xu et al., 2020). During the intricate process of cell migration, it is imperative for cells to accurately perceive directional cues in order to initiate movement, specifically

towards the correct direction (Fu et al., 2019). DCEFs have been proved to be a highly effective means of facilitating directed cell migration in embryonic development and wound healing, surpassing alternative extracellular signals (Nuccitelli, 2003; Zhao et al., 2006). Here, we have successfully observed the electrotaxis of SCAP, which exhibited migration towards the anode for the first time. This finding serves as significant evidence for the directional guidance of stem cells towards the site of damaged dentine tissue, a crucial prerequisite for dentine regeneration (Suzuki et al., 2011). In addition, it is imperative for external stimuli to maintain a delicate equilibrium between the proliferation and differentiation of SCAP, as these cellular processes commonly demonstrate a notable negative correlation (Ruijtenberg & van den Heuvel, 2016). In this study, it was observed that different intensities of DCEFs had distinct effects on the biological behaviours of SCAP. We confirmed that the intensity of 100 mV/mm of DCEFs significantly enhanced cell proliferation, whilst the migration and odontogenic differentiation potentials of SCAP were maximized at the intensity of 200 mV/mm. Whereas, the proliferation and migration of SCAP decreased when subjected to DCEFs with the intensity of 300 mV/mm. We speculated the damage phenomenon might be attributed to membrane impairment, which is caused by the substantial escalation of toxicity products and thermogenesis with the increase of electric field strength (Chen & Wu, 2006). Additionally, the rise in reactive oxygen species (ROS), the influx of calcium ions ( $\text{Ca}^{2+}$ ) and the depletion of adenosine triphosphate (ATP) are believed to contribute to deleterious effects on cell metabolism (Batista Napotnik et al., 2021; Ren et al., 2019). On the other hand, it has been documented that injured tissue produces significantly greater electrical currents compared to healthy tissue (Fish & Geddes, 2009; Reid & Zhao, 2014). This phenomenon can be attributed to several underlying mechanisms, including the disruption of the damaged cell membrane in injured tissue, the migration of inflammatory cells to the injury site, and the enhanced metabolic activity and ion transport associated with cell division and protein synthesis necessary for tissue repair. The present results may inspire the novel strategy of SCAP-mediated dentine regeneration through the precise modulation of DCEFs at specific time points. Specifically, a strength of 100 mV/mm is recommended for promoting cell proliferation, whilst a strength of 200 mV/mm is suggested for facilitating cell migration and odontogenic differentiation, based on the specific requirements of the regenerative process. An electric field strength of 300 mV/mm may serve as a valuable tool for simulating and investigating the mechanisms underlying periapical tissue injury.

The exact mechanisms underlying cellular recognition and response to electric fields remain poorly understood, although some studies have implicated that some cell surface

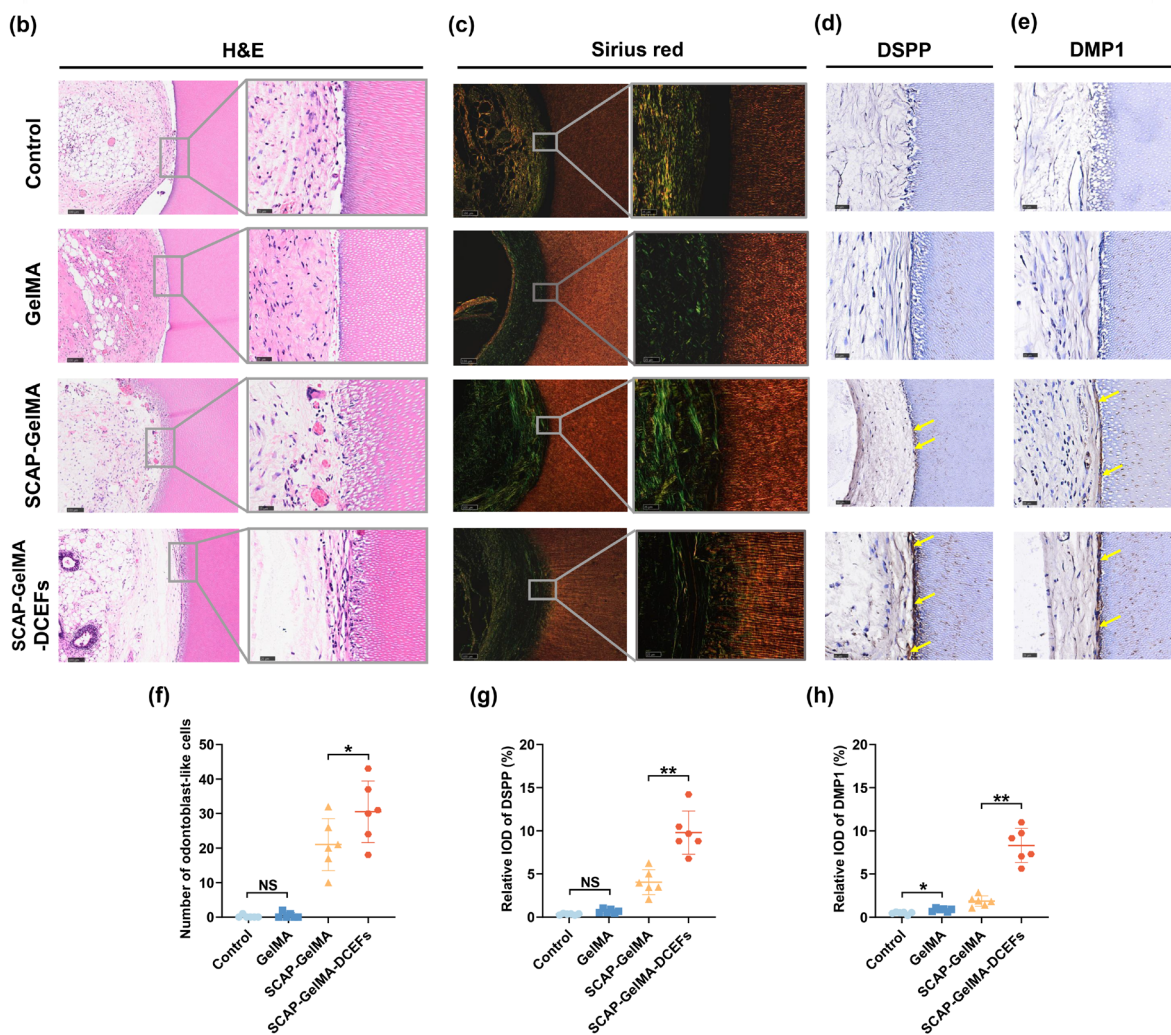
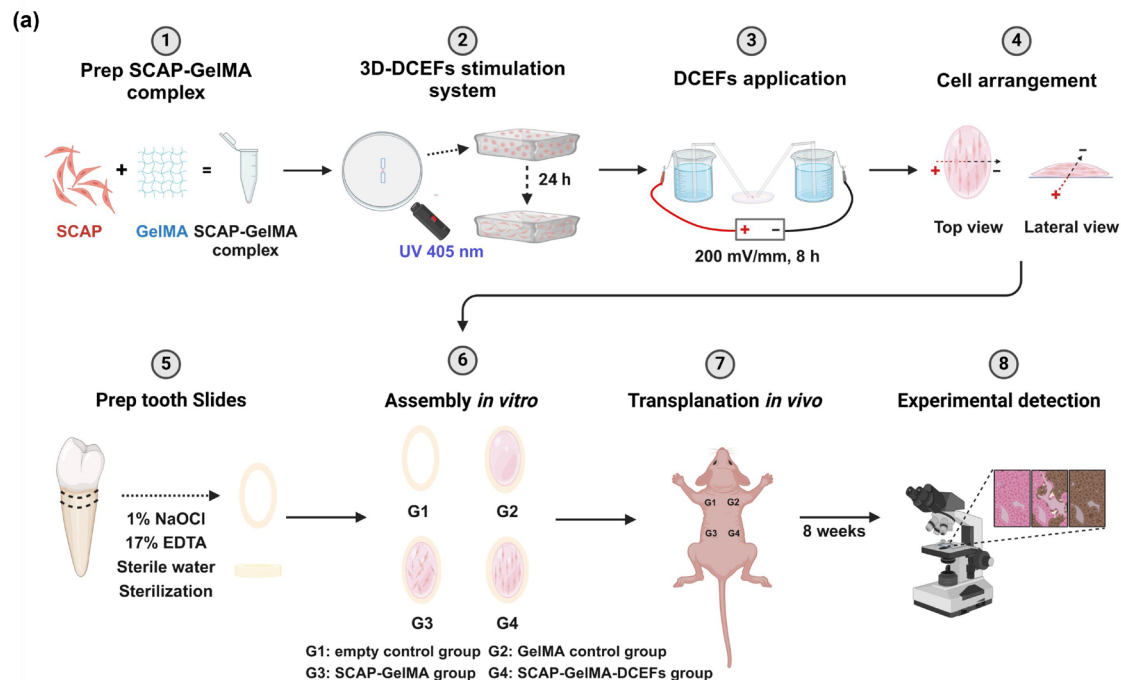


**FIGURE 6** DCEFs boosted dentineogenesis of SCAP in vivo. (a) Schematic diagram of in vivo experiments (Created with BioRender.com). (b, c) Representative images of H&E staining and Sirius red staining. (d, e) Immunohistochemistry staining images of DSPP and DMP1 (yellow arrows indicate newly formed dentine-like tissues composed of DSPP or DMP1 positive staining cells). (f) Quantification number of odontoblast-like cells per unit field. (g, h) The expression levels of DSPP and DMP1 detected by immunohistochemistry were statistically quantified (NS:  $p > .05$ ,  $*p < .05$ ,  $**p < .01$ ,  $n = 6$ / group).

receptors and ion channels could be involved (Ma et al., 2023; Tsai et al., 2013). In this study, we confirmed that DCEFs induced cytoskeleton remodelling, with a particular emphasis on the interplay between changes in cell shape, alignment, and function. Our experimental findings revealed that 67% of cells aligned perpendicular to the electrical field vector and adopted a fence-like structure following DCEF stimulation, closely resembling the differentiation process of SCAP into odontoblasts under physiological conditions. Moreover, the positioning of the Golgi apparatus in relation to the nucleus exhibited increased organization following DCEFs loading, mirroring a similar phenomenon observed during the development and maturation of odontoblasts where the Golgi localized on the opposite side of the nucleus. The arrangement of the Golgi apparatus induced by DCEFs may be attributed to the formation of organized dentine-like tissue, as secretion involves the directed transportation of Golgi-derived vesicles to the cell periphery followed by exocytosis (Schuster et al., 2012). Aligned cells demonstrate an increased tendency to penetrate open dentine tubules (Ha et al., 2020). When these cells are systematically organized, their longitudinal axes align with the orientation of the dentine tubules, enabling them to more effectively utilize their intrinsic motility and the physicochemical gradients of the tubules. This alignment, in contrast to disordered cells, facilitates a more efficient ingress into the dentine tubules, resembling a “queuing” mechanism. The intricate interconnections and interactions among the cells enhance their anchorage within the tubules, thereby establishing a relatively stable cellular community capable of performing secretory functions (Martín-de-Llano et al., 2019). Consequently, challenges that need to be addressed include optimizing the construction of 3D in vitro models, anchoring pre-differentiated and electrically stimulated SCAP within scaffold materials, and ensuring their precise alignment. In contrast to odontoblasts, which undergo a series of sequential and reciprocal epithelial-mesenchymal interactions, SCAP received singular external directional stimulation from DCEFs in this experiment, resulting in Golgi positioning either above or below the nucleus. Our study has demonstrated that DCEFs play a significant role in promoting stem cell-mediated biomimetic dentine tissue repair, offering a promising direction for further research on odontoblast differentiation in vitro and filling the gap of the 2D biomimetic platform for studying odontoblast polarization (Chang et al., 2021).

Otherwise, in accordance with the established relationship between pulp and dentine, the pulp–dentine complex is acknowledged as an integrated entity, wherein DCEFs from injured periapical tissues influence both dentine and neural structures. The trans-differentiation of MSCs into neurons via electrical stimulation has been previously validated and enhanced (Liang et al., 2022; Tai et al., 2023). A large number of studies have provided evidence that regenerative endodontic procedures can lead to dentine re-establishment, accompanied by neurogenesis (Diogenes, 2020). Whilst the role of neurotrophic factors in tooth development is well documented (Fried et al., 2007) and dentine matrix proteins (DMPs) derived from extracted human teeth have been found to contain various neurotrophic factors, including nerve growth factor, brain-derived neurotrophic factor, glial cell line-derived neurotrophic factor, neurotrophin-3, and neurotrophin-4 (Austah et al., 2019), the precise mechanisms governing the mutual regulation between dentine and nerve tissue remain unclear. Considering the critical role of innervation in pulp homeostasis, repair, and regeneration, it is imperative to conduct further research to expand the current understanding of the functionality of DCEFs.

## CONCLUSIONS

In summary, we have successfully adapted conventional 2D and advanced 3D DCEFs stimulating models, providing clear experimental support for the effect of DCEFs on migration, proliferation, and odontogenic differentiation of SCAP for the first time. The results provided a basis and theoretical rationale for further application of DCEFs in tubular dentine regeneration in the dentine-pulp complex regeneration. For translational application, this study serves as an important foundation for the development of a novel pulp capping agent, electrical periapical stimulation device, and strategy for whole-tooth regeneration. However, this method is currently in its nascent stage and undergoing preliminary exploration. Our future work will involve proteomics analysis to investigate the influence of DCEFs on the functional protein expression profiles of SCAP. In addition, we are currently investigating the potential long-term effects of endogenous current on the GelMA-SCAP complex in injured teeth. Most importantly, the outcomes of this study will be utilized to enhance the dependability



of the results obtained from large-animal models, facilitating the future application of DCEFs in the regeneration of tubular dentine within the pulp-dentine complex.

## AUTHOR CONTRIBUTIONS

Xiaolin Li was involved in the conceptual design of the work, analysis, and interpretation of data, and writing the original draft. Sanjun Zhao performed the experiment and analysis. Yao Liu and Yu Gu performed the analysis and interpretation of data. Lihong Qiu was involved in the conceptual design of the work. Xu Chen, Alastair J Sloan, and Bing Song were involved in the conceptual design of the work and critically revised the manuscript. All authors reviewed and approved the manuscript.

## ACKNOWLEDGEMENTS

This research was supported by the National Natural Science Foundation of China (Grant No. T2350710233, 82060355), the National Key R&D Program of China (2024YFF206402, 2023YFC2508200), tShenzhen Science and Technology Program (Grant No. JCYJ20220818101404009) and the China Scholarship Council (Grant No. CSC201908210295).

## CONFLICT OF INTEREST STATEMENT

The authors have stated explicitly that there are no conflicts of interest in connection with this article.

## DATA AVAILABILITY STATEMENT

All data are available from the corresponding author upon reasonable request.

## ETHICS STATEMENT

The study was approved by the Ethics Committee of the School and Hospital of Stomatology, China Medical University (No. 201315 and No. G2018009). The protocol for the animal experiment was approved by the Institutional Animal Care and Use Committee of China Medical University (No. CMU2021211).

## ORCID

Xiaolin Li  <https://orcid.org/0000-0002-5454-3065>

Yao Liu  <https://orcid.org/0000-0001-9794-1314>

Xu Chen  <https://orcid.org/0000-0002-2158-8320>

Alastair J. Sloan  <https://orcid.org/0000-0002-1791-0903>

Bing Song  <https://orcid.org/0000-0001-9356-2333>

## REFERENCES

- Al Hezaimi, K., Berdan, Y. & Rotstein, I. (2023) Assessment of dentine mineral density of human teeth using micro-computed tomography in two kilovoltage levels. *Odontology*, 111(4), 904–909.
- Austah, O., Widbiller, M., Tomson, P.L. & Diogenes, A. (2019) Expression of neurotrophic factors in human dentine and their regulation of trigeminal neurite outgrowth. *Journal of Endodontics*, 45(4), 414–419.
- Balmer, T.W., Vesztergom, S., Broekmann, P., Stahel, A. & Büchler, P. (2018) Characterization of the electrical conductivity of bone and its correlation to osseous structure. *Scientific Reports*, 8(1), 8601.
- Batista Napotnik, T., Polajžer, T. & Miklavčič, D. (2021) Cell death due to electroporation—a review. *Bioelectrochemistry Amsterdam, Netherlands*, 141, 107871.
- Chang, B., Ma, C., Feng, J., Svoboda, K.K.H. & Liu, X. (2021) Dental pulp stem cell polarization: effects of biophysical factors. *Journal of Dental Research*, 100(10), 1153–1160.
- Chen, C., Bai, X., Ding, Y. & Lee, I.S. (2019) Electrical stimulation as a novel tool for regulating cell behavior in tissue engineering. *Biomaterials Research*, 23, 25.
- Chen, W. & Wu, W.H. (2006) Electric field-induced changes in membrane proteins charge movement currents. *Burns: Journal of the International Society for Burn Injuries*, 32(7), 833–841.
- Ding, G., Wang, W., Liu, Y., An, Y., Zhang, C., Shi, S. et al. (2010) Effect of cryopreservation on biological and immunological properties of stem cells from apical papilla. *Journal of Cellular Physiology*, 223(2), 415–422.
- Diogenes, A. (2020) Trigeminal sensory neurons and pulp regeneration. *Journal of Endodontics*, 46(9S), S71–S80.
- Fish, R.M. & Geddes, L.A. (2009) Conduction of electrical current to and through the human body: a review. *Eplasty*, 9, e44.
- Fried, K., Lillesaar, C., Sime, W., Kaukua, N. & Patarroyo, M. (2007) Target finding of pain nerve fibres: neural growth mechanisms in the tooth pulp. *Physiology & Behavior*, 92(1–2), 40–45.
- Fu, X., Liu, G., Halim, A., Ju, Y., Luo, Q. & Song, A.G. (2019) Mesenchymal stem cell migration and tissue repair. *Cells*, 8(8), 784.
- Grimm, D., Wehland, M., Pietsch, J., Aleshcheva, G., Wise, P., van Loon, J. et al. (2014) Growing tissues in real and simulated microgravity: new methods for tissue engineering. *Tissue Engineering. Part B, Reviews*, 20(6), 555–566.
- Ha, M., Athirasala, A., Tahayeri, A., Menezes, P.P. & Bertassoni, L.E. (2020) Micropatterned hydrogels and cell alignment enhance the odontogenic potential of stem cells from apical papilla in vitro. *Dental Materials: Official Publication of the Academy of Dental Materials*, 36(1), 88–96.
- Han, Y.L., Wang, S., Zhang, X., Li, Y., Huang, G., Qi, H. et al. (2014) Engineering physical microenvironment for stem cell based regenerative medicine. *Drug Discovery Today*, 19(6), 763–773.
- Hart, F.X. & Palisano, J.R. (2017) *The application of electric fields in biology and medicine. Electric field: the application of electric fields in biology and medicine*. London, United Kingdom: InTechOpen Press, p. 322.
- Huang, G.T., Gronthos, S. & Shi, S. (2009) Mesenchymal stem cells derived from dental tissues vs. those from other sources: their biology and role in regenerative medicine. *Journal of Dental Research*, 88(9), 792–806.
- Huang, G.T., Liu, J., Zhu, X., Yu, Z., Li, D., Chen, C.A. et al. (2020) Pulp/dentine regeneration: it should be complicated. *Journal of Endodontics*, 46(9S), S128–S134.
- Jung, C., Kim, S., Sun, T., Cho, Y.B. & Song, M. (2019) Pulp-dentine regeneration: current approaches and challenges. *Journal of Tissue Engineering*, 10, 2041731418819263.
- Khayat, A., Monteiro, N., Smith, E.E., Pagni, S., Zhang, W., Khademosseini, A. et al. (2017) GelMA-encapsulated hDPSCs



- and HUVECs for dental pulp regeneration. *Journal of Dental Research*, 96(2), 192–199.
- Leppik, L., Oliveira, K.M.C., Bhavsar, M.B. & Barker, J.H. (2020) Electrical stimulation in bone tissue engineering treatments. *European Journal of Trauma and Emergency Surgery: Official Publication of the European Trauma Society*, 46(2), 231–244.
- Li, M., Ma, L., Song, B., Yu, D., Xiao, M., Mei, X. et al. (2018) Cdc42 is essential for the polarized movement and adhesion of human dental pulp stem cells. *Archives of Oral Biology*, 85, 104–112.
- Liang, L., Liu, C., Cai, P., Han, S., Zhang, R., Ren, N. et al. (2022) Highly specific differentiation of MSCs into neurons directed by local electrical stimuli triggered wirelessly by electromagnetic induction nanogenerator. *Nano Energy*, 100, 107483.
- Liu, Y., Zhuang, X., Yu, S., Yang, N., Zeng, J., Liu, X. et al. (2021) Exosomes derived from stem cells from apical papilla promote craniofacial soft tissue regeneration by enhancing Cdc42-mediated vascularization. *Stem Cell Research & Therapy*, 12(1), 76.
- Ma, T., Ding, Q., Liu, C. & Wu, H. (2023) Electromagnetic fields regulate calcium-mediated cell fate of stem cells: osteogenesis, chondrogenesis and apoptosis. *Stem Cell Research & Therapy*, 14(1), 133.
- Martín-de-Llano, J.J., Mata, M., Peydró, S., Peydró, A. & Carda, C. (2019) Dentine tubule orientation determines odontoblastic differentiation in vitro: a morphological study. *PLoS One*, 14(5), e0215780.
- McCaig, C.D., Rajnicek, A.M., Song, B. & Zhao, M. (2005) Controlling cell behavior electrically: current views and future potential. *Physiological Reviews*, 85(3), 943–978.
- Nagendrababu, V., Murray, P. E., Ordinola-Zapata, R., Peters, O. A., Rôças, I. N., Siqueira, Jr., J. F. et al. (2021) PRILE 2021 guidelines for reporting laboratory studies in Endodontology: a consensus-based development. *International Endodontic Journal*, 54(9), 1482–1490.
- Nuccitelli R. (2003) A role for endogenous electric fields in wound healing. *Current Topics in Developmental Biology*, 58, 1–26.
- Piva, E., Silva, A.F. & Nör, J.E. (2014) Functionalized scaffolds to control dental pulp stem cell fate. *Journal of Endodontics*, 40(4 Suppl), S33–S40.
- Reid, B., Nuccitelli, R. & Zhao, M. (2007) Non-invasive measurement of bioelectric currents with a vibrating probe. *Nature Protocols*, 2(3), 661–669.
- Reid, B. & Zhao, M. (2014) The electrical response to injury: molecular mechanisms and wound healing. *Advances in Wound Care*, 3(2), 184–201.
- Ren, X., Sun, H., Liu, J., Guo, X., Huang, J., Jiang, X. et al. (2019) Keratinocyte electrotaxis induced by physiological pulsed direct current electric fields. *Bioelectrochemistry* Amsterdam, Netherlands, 127, 113–124.
- Ruijtenberg, S. & van den Heuvel, S. (2016) Coordinating cell proliferation and differentiation: antagonism between cell cycle regulators and cell type-specific gene expression. *Cell Cycle (Georgetown, Texas)*, 15(2), 196–212.
- Schuster, M., Treitschke, S., Kilaru, S., Molloy, J., Harmer, N.J. & Steinberg, G. (2012) Myosin-5, kinesin-1 and myosin-17 cooperate in secretion of fungal chitin synthase. *The EMBO Journal*, 31(1), 214–227.
- Song, B., Gu, Y., Pu, J., Reid, B., Zhao, Z. & Zhao, M. (2007) Application of direct current electric fields to cells and tissues in vitro and modulation of wound electric field in vivo. *Nature Protocols*, 2(6), 1479–1489.
- Sui, B., Chen, C., Kou, X., Li, B., Xuan, K., Shi, S. et al. (2019) Pulp stem cell-mediated functional pulp regeneration. *Journal of Dental Research*, 98(1), 27–35.
- Suzuki, T., Lee, C.H., Chen, M., Zhao, W., Fu, S.Y., Qi, J.J. et al. (2011) Induced migration of dental pulp stem cells for in vivo pulp regeneration. *Journal of Dental Research*, 90(8), 1013–1018.
- Tai, Y., Tonmoy, T.I., Win, S., Brinkley, N.T., Park, B.H. & Nam, J. (2023) Enhanced peripheral nerve regeneration by mechano-electrical stimulation. *npj Regenerative Medicine*, 8(1), 57.
- Tibúrcio-Machado, C.S., Michelon, C., Zanatta, F.B., Gomes, M.S., Marin, J.A. & Bier, C.A. (2021) The global prevalence of apical periodontitis: a systematic review and meta-analysis. *International Endodontic Journal*, 54(5), 712–735.
- Tsai, C.H., Lin, B.J. & Chao, P.H. (2013)  $\alpha 2\beta 1$  integrin and RhoA mediates electric field-induced ligament fibroblast migration directionality. *Journal of Orthopaedic Research: Official Publication of the Orthopaedic Research Society*, 31(2), 322–327.
- Xie, W., Wei, X., Kang, H., Jiang, H., Chu, Z., Lin, Y. et al. (2023) Static and dynamic: evolving biomaterial mechanical properties to control cellular Mechanotransduction. *Advanced Science (Weinheim, Baden-Wurttemberg, Germany)*, 10(9), e2204594.
- Xu, X.Y., Tian, B.M., Xia, Y., Xia, Y.L., Li, X., Zhou, H. et al. (2020) Exosomes derived from P2X7 receptor gene-modified cells rescue inflammation-compromised periodontal ligament stem cells from dysfunction. *Stem Cells Translational Medicine*, 9(11), 1414–1430.
- Yasui, T., Mabuchi, Y., Morikawa, S., Onizawa, K., Akazawa, C., Nakagawa, T. et al. (2017) Isolation of dental pulp stem cells with high osteogenic potential. *Inflammation and Regeneration*, 37, 8.
- Yin, J., Xu, J., Cheng, R., Shao, M., Qin, Y., Yang, H. et al. (2021) Role of connexin 43 in odontoblastic differentiation and structural maintenance in pulp damage repair. *International Journal of Oral Science*, 13(1), 1.
- Zhao, M., Song, B., Pu, J., Wada, T., Reid, B., Tai, G. et al. (2006) Electrical signals control wound healing through phosphatidylinositol-3-OH kinase-gamma and PTEN. *Nature*, 442(7101), 457–460.

## SUPPORTING INFORMATION

Additional supporting information can be found online in the Supporting Information section at the end of this article.

**How to cite this article:** Li, X., Zhao, S., Liu, Y., Gu, Y., Qiu, L., Chen, X. et al. (2025) Electric field promoted odontogenic differentiation of stem cells from apical papilla by remodelling cytoskeleton. *International Endodontic Journal*, 58, 873–889. Available from: <https://doi.org/10.1111/iej.14213>